Medical Hypotheses 130 (2019) 109277

Contents lists available at ScienceDirect

Medical Hypotheses

journal homepage: www.elsevier.com/locate/mehy

Broadening the horizon: Integrative pharmacophore-based and cheminformatics screening of novel chemical modulators of mitochondria ATP synthase towards interventive Alzheimer's disease therapy

Iwuchukwu A. Emmanuel*, Fisayo Olotu, Clement Agoni, Mahmoud E.S. Soliman*

Molecular Bio-computation and Drug Design Laboratory, School of Health Sciences, University of KwaZulu-Natal, Westville Campus, Durban 4001, South Africa

ARTICLE INFO

Keywords:
J147
Pharmacophore-based virtual screening
Per-residue energy decomposition
ATP5A
Pharmacokinetics

ABSTRACT

The proven efficacy of J147 in the treatment of Alzheimer's disease (AD) has been emphatic, particularly since its selective modulatory roles towards mitochondrial ATP synthase (*m*ATPase) were defined. This prospect, if methodically probed, could further pave way for the discovery of novel anti-AD drugs with improved pharmacokinetics and therapeutic potential. To this effect, for the first time, we employed a four-step paradigm that integrated our in-house per-residue energy decomposition (PRED) protocol coupled with molecular dynamics, cheminformatics and analytical binding free energy methods. This was geared towards the screening and identification of new leads that exhibit modulatory potentials towards *m*ATPase in a J147-similar pattern. Interestingly, from a large-scale library of compounds, we funnelled down on three potential hits that demonstrated selective and high-affinity binding activities towards α-F1-ATP synthase (ATP5A) relative to J147. Moreover, these compounds exhibited higher binding propensity with a differential **ΔGs** greater than −1 kcal/mol comparative to J147, and also elicited distinct modulatory effects on ATP5A domain structures. More interestingly, per-residue pharmacophore modeling of these lead compounds revealed similar interactive patterns with crucial residues at the α-site region of ATP5A characterized by high energy contributions based on binding complementarity. Recurrent target residues involved in high-affinity interactions with the hit molecules relative to J147 include Arg1112 and Gln426. Furthermore, assessments of pharmacokinetics revealed that the lead compounds were highly drug-like with minimal violations of the Lipinski's rule of five. As developed in this study, the most extrapolative pharmacophore model of the selected hits encompassed three electron donors and one electron acceptor. We speculate that these findings will be fundamental to the reformation of anti-AD drug discovery procedures.

Introduction

Alzheimer's disease (AD) is a multifactorial neurodegenerative disease and a leading cause of death around the world with vast majority of the patients being individuals around the age of 65 years and above [1,2]. AD is characterized by elevated levels of soluble and insoluble amyloid-β (Aβ), mainly in the form of Aβ42 in amyloid plaques and Aβ40 in amyloid angiopathy [3]. The amyloid hypothesis suggests that AD is caused by an inequality between Aβ production and clearance [3,4], contributing to increased levels of Aβ in diverse forms in the Central Nervous System (CNS). High levels of Aβ initiate a cascade of events that results in neuronal damage and death, which in turn manifest as progressive clinical dementia of the Alzheimer type [3,5].

Current treatment options for AD have been directed at symptoms and are usually involved in modulation of transmitter disturbance [6]. Three cholinesterase inhibitors (CIs) currently approved and available for the treatment of mild to moderate AD include Aricept, Exelon, and Razadyne [7]. Memantine is a non-competitive antagonist of N-methyl-D-aspartate (NMDA) receptor that has also been employed in the treatment of moderate to severe AD [6]. These drugs, together with other available agents improves the cognitive decline and memory impairment associated with AD [7].

Recent advancements in anti-AD drug discovery has led to the identification of J147, a neurotrophic compound derived from curcumin, which is shown to reverse cognitive impairment in age-related neurodegenerative diseases such as AD [8–10]. J147 was able to improve memory in aging mice plagued with AD while also demonstrating the ability to rescue cognitive deficits at a late disease stage [9]. It also

* Corresponding author.
E-mail address: soliman@ukzn.ac.za (M.E.S. Soliman).
URL: http://soliman.ukzn.ac.za (M.E.S. Soliman).

https://doi.org/10.1016/j.mehy.2019.109277
Received 5 March 2019; Received in revised form 3 June 2019; Accepted 10 June 2019

promoted the functions of proteins which are important for learning and memory [9]. Due to the ability of J147 to halt and maybe reverse the progression of disease in symptomatic model animals complemented by an immediate improvement in cognition, J147 has been widely accepted for its therapeutic potential as an anti-AD drug [9]. With regards to its therapeutic activity, recent reports revealed that J147 targets mitochondrial α-F_1-ATP synthase (ATP5A) [11,12]. Mitochondrial ATP synthase (*m*ATP synthase) also called F_oF_1 ATPase comprises two defined entities which are the F_1 domain and F_0 domain [13]. The F_0 domain which is located at the inner mitochondrial membrane; deriving its name F0-ATP synthase from binding to oligomycin [14,15]. F1 domain consists of three α and β subunits ($\alpha_3\beta_3$) respectively and the additional γ, δ and ε subunits are one [13,16]. Both the α and β subunits binds nucleotide but only the three respective β subunit are catalytically active [17]. *m*ATP synthase is associated with multiple cellular processes and is ubiquitous enzyme that is highly conserved in human life thus making it an interesting drug target harbouring about twelve inhibitor binding sites [18,19]. It is therefore necessary to explore avenues created by the discovery of this novel drug and target protein to facilitate the identification of other active molecules that are able to modulate the activity of *m*ATP synthase relative to AD treatment.

The limited number of effective drugs for AD treatment as well as associated side effects necessitates a continuous search for more viable therapeutic options. The advent of computer-aided drug design has enhanced and hastened drug discovery processes particularly due to its ability to identify and repurpose existing molecules for new pathogenic targets thereby saving enormous time and cost, contrary to the conventional methods which entails drug design from the scratch [20]. Based on the well-defined allosteric inhibitory mechanisms of J147 against α-F1-ATP synthase, this study employs integrative computational methods to identify potential anti-AD inhibitors with similar or enhanced inhibitory properties, which could typify a cohort of novel α-F1-ATP synthase inhibitors. To this effect, we generated a pharmacophore model based on the binding landscape as well as the structure-activity relationship of J147 in complex with α-F1-ATP synthase at the α-allosteric domain using our in-house established per-residue energy decomposition (PRED) protocol [21,22]. The PRED protocol was used to predict essential moieties of J147 based on energy contributions of key amino acid residues of ATP5A α-site that interacted with J147. Afterwards, we screened for possible hit compounds from large compound libraries based on our defined pharmacophore model. We further explored the pharmacokinetic properties of these hit compounds as well as their impact on the structural dynamics of α-F1-ATP synthase relative to J147. The generated pharmacophore model would further assist medicinal chemists in the design of highly effective small molecules inhibitor for AD therapy. Hits identified in this report could also be further investigated using applicable *in vitro* and *in vivo* methods to validate their inherent therapeutic potencies towards α-F1-ATP synthase in the treatment of AD or AD-related diseases.

Hypothesis

The present study hypothesized that through the screening of the ZINC database by the employment of ligand-based drug discovery and structure-based drug discovery, newer ligands which possesses better inhibitory potential against mATP synthase which is a novel therapeutic target implicated in Alzheimer's disease can be discovered. This mATP synthase is a highly conserved protein and is ubiquitous in the human body, this therefore is an added advantage as targeting this protein will bring rapid control to the menace of Alzheimer's disease. The present hypothesis was tested by employing *in-silico* molecular modelling wherein the conformational dynamics of the protein when bound with ligands, the per-residue energy decomposition and the physicochemical parameters could provide an insight in understanding the hypothesis.

Computational methods

Measure of drug likeliness

SwissADME [23], an online platform was used to determine the physicochemical descriptors, pharmacokinetic properties and drug-like properties of J147. The lipophilicity and polarity of J147 was measured with the "brain or intestinal estimated permeation, (BOILED-Egg)" method [23,24].

System preparation of J147-mATP synthase complexes

Due to lack of 3D crystal structure for human ATP synthase, a homology model was built using bovine mATP synthase crystal structure with PDB code 1BMF as template [25]. The template bovine mATP synthase possessed a sequence identity of 97.15% with human ATP synthase. The protocol for building the homology was in accordance with in-house protocols as employed in our previous reports [26,27]. The built 3D structure of human ATP synthase was validated using PROCHECK [28], RAMPAGE [29] and VERIFY-3D [30] online platforms. All non-standard atoms including co-crystalized solvent molecules and ligands were deleted from the target protein. System preparation was performed using The UCSF Chimera Graphical User Interface (GUI) [31]. By removing all other subunits except the $\alpha_3\beta_3\gamma$ subunit. This was done to minimize computational cost considering the large size of the entire human ATP synthase structure (~3880 residues). The J147 binding site region on ATP5A (α_E) was mapped out by superposing with α_{DP} (with ADP in the allosteric pocket), after which the gridbox was used to obtain the analogous coordinates with AutoDock Vina [32]. Prior to molecular docking, the 2D structure of J147, was retrieved from PubChem database and prepared using Avogadro software [33]. The pdbqt formats of the ligands and target protein were automatically generated by the AutoDock Vina extension of UCSF Chimera while the optimal binding energy of the ligand and the corresponding poses was obtained. The size of the grid box was determined using Autodock Vina with size dimension x = 9.1646, y = 12.5126, z = 11.1492 and centred at x = 1.2393, y = 11.0932, z = 2.4829.

Molecular dynamic (MD) simulations

The GPU version of the PMEMD engine provided with the Amber 18 package was used for the MD simulation. FF14SB [34] variant of Amber force field was used to determine the protein system parameters. Atomic partial charges for the ligands was generated by ANTECHAMBER [35] using the Restrained Electrostatic Potential (RESP) and the General Amber Force Field (GAFF) procedures. Hydrogen atoms were added to the systems as well as Na+ and Cl− counter ions for neutralization using the Leap module of Amber 18. An orthorhombic box of TIP3P water molecules was used to suspend the systems such that all atoms were within an 8 Å box edge. Initial minimization of 2000 steps was performed with an applied restraint potential of 500 kcal/mol$Å^{-2}$ for all the systems. Another full minimization of 1000 step was further performed by conjugate gradients algorithm without restrain. A continuous but slow and steady heating MD simulation from 0 K to 300 K was done for 50 ps, in such a manner that the systems maintained a fixed number of atoms and fixed volume, i.e., a canonical ensemble (NVT). A potential harmonic restraint of 10 kcal/mol $Å^2$ and collision frequency of 1.0 ps^{-1} was imposed on the solutes within the system. After an equilibration estimating 500 ps of each system was carried out, the operating temperature was maintained at 300 K. More distinctive qualities such as number of atoms and pressure were kept constant mimicking an isobaric-isothermal ensemble (NPT). Berendsen barostat was employed to maintain the pressure of the systems at 1 bar. MD phase was carried out at 300 K for 100 ns with a time step of 2 fs using the canonical ensemble (amount of substance volume temperature

[NVT]) and particle mesh Ewald method [36] with a direct space and vdW cut-off of 12 Å was used for the calculation of electrostatic interactions. SHAKE algorithm was employed to constrict the bonds of hydrogen atoms in each simulation. The simulations tallied with isobaric-isothermal ensemble (NPT), with randomized seeding, constant pressure of 1 bar maintained by the Berendsen barostat, a pressure coupling constant of 2 ps, a temperature of 300 K and Langevin thermostat with collision frequency of 1.0 ps^{-2}. Coordinates were saved every 1 ps and the trajectories were analysed every 1 ps using the PTRAJ and CPPTRAJ module employed in Amber18.

Binding free energy calculations

The binding free energy of all the simulated complexes were calculated using the Molecular Mechanics Generalized Born Surface Area (MM/GBSA) method [37]. The mean binding free energy over 2000 snapshots were extracted from the 20 ns trajectory. The following set of equations describes the calculation of the binding-free energy (ΔG):

$$\Delta G_{bind} = G_{complex} - G_{receptor} - G_{ligand} \quad (1)$$

$$\Delta G_{bind} = E_{gas} + G_{sol} - TS \quad (2)$$

$$E_{gas} = E_{int} + E_{vdw} + E_{ele} \quad (3)$$

$$G_{sol} = G_{GB} + G_{SA} \quad (4)$$

$$G_{SA} = \gamma SASA \quad (5)$$

The E_{gas} term represents the gas phase energy, which comprises the internal energy E_{int}; Coulomb energy E_{ele} and the van der Waals energies; E_{vdw}. The FF14SB force field terms was used to estimate the E_{gas}. The energy contribution from the polar states, G_{GB} and non-polar states, G_{SA} was used to estimate solvation free energy G_{sol}. Solvent accessible surface area (SASA) was employed to determine the non-polar solvation energy, SA using a water probe radius of 1.4 Å, while the polar solvation, G_{GB}, contribution was determined by solving the GB equation, where the total entropy of the solute and temperature was represented by S and T respectively. To obtain the contribution of each residue to the total binding free energy profile between the inhibitors and ATP synthase, per residue free energy decomposition was carried out at the atomic level for imperative residues using the MM/GBSA method in Amber 14.

Pharmacophore model creation

In order to obtain the bound conformation of the ligand, the inhibitor J147 was first simulated at the allosteric site of αF_1-ATPase for 20 ns. J147 has been experimentally reported to bind ATP5A and modulate the activity of *m*ATP synthase relative to the treatment of AD, as such, its selective interaction with αF1-ATPase serves as the basis for pharmacophoric development as proposed in this report [11]. The amino acids that contributed the most towards ligand binding were determined by applying per-residue energy decomposition analysis. The model was then constructed by choosing pharmacophoric moieties that interacted with high energy contributing residues. The constructed model was added to ZINCPharmer [23,24] with distinct criteria (molecular weight of < 500 Da, hydrogen bond donors < 5, hydrogen bond acceptors < 10 and rotatable bonds < 5) to screen the ZINC database [25] for potential inhibitors that contained those pharmacophoric moieties. Non-drug like hits were filtered using Lipinski's rule of five [26,27] and ADMET properties [28].

Structure-based virtual screening

The identified drug-like hits from our protocol were further subjected to structure-based virtual screening. Molecular docking was performed to differentiate ligands based on their geometric characteristics that permit binding at enzyme's active or allosteric site [38]. The docking estimations were carried out using Autodock Vina [32]. Gasteiger partial chargers were assigned and the Autodock atom types were defined using the Autodock Graphical user interface supplied by MGL tools [39]. The docked conformations were produced using the Lamarckian Genetic Algorithm [40]. Maestro was employed in converting the ligand SDF file to the mol2 format and the ligands were further converted into pdbqt formats required for docking with the aid of Raccoon. Autodock Vina was used in defining the gridbox. The calculation reports for the various ligand conformations in their respective complex were analysed to obtain affinity energy (kcal/mol). During the docking process, a maximum of 9 conformers was considered for each compound. After screening, molecular docking and filtering, three ligands with the highest affinity towards the target protein was selected from the library. The docked conformation of the compounds complexed with ATP synthase were generated and visualized in the ViewDock plugin-integrated Chimera as was done with the reference ligand, J147[41]. The compounds were ranked in order of binding affinity from greatest to smallest. To create a pharmacophore model based on docked system of a ligands complexed with ATP synthase, MD simulation and post-MD analysis were carried out on the docked complexes.

Validation of docking approach

Experiences in the past have proven that docking may result in the best geometric conformation of the docked complex, however, short molecular dynamic simulations may not be able to maintain the stability of the complex and therefore lead to the molecules being disorientated. Thus, to validate the approach applied in our study, the three most favourable ATP synthase complexes were subjected to further molecular dynamics studies using the same procedure as reported in the molecular dynamics section, but in case the molecular dynamics was run for 100 ns and J147, the reference ligand molecular dynamics was also extended to 100 ns.

Results and discussion

Validation of 3D model of mATP synthase of human

The homology model of the human ATP synthase employed in this report was generated based on a template structure of bovine mATP synthase [25] with a sequence identity of 97.15%. The structural validation of the our model was performed using Ramachandran plot incorporated on RAMPAGE online platform which showed that 95.5% of the amino acid residues in the model are in the favour region, 3.9% appeared in the allowed region whereas the outlier region has 0.6% of the residues as shown in Fig. S1. This also gave insights into the accuracy of the dihedral angles and backbone in three-dimensional area. A follow-up validation of the model was also performed using the PROSA web server in terms of Z-score. PROSA web server provided insights on whether the homology model was within acceptable X-ray and NMR studies. The modelled ATP synthase showcased a Z-score of −2.87 as indicated in the Supplementary Table S1. The Z-score recorded from PROSA web server suggested a good quality model as shown in plot in Fig. S2. The empirical and energetic techniques applied by Verify_3D was also used to estimate the quality of the model, which provides average data points of individual residues. The modelled *m*ATP synthase exhibited a Verify-3D score of 86.39% with > 0.2 score. In addition to the validation techniques employed, the quality of our model was further evaluated using the PROCHECK, whose summary is presented in Supplementary fig. S3. It indicates that 90.7% are in the most favoured regions, 8.4% located in the additional allowed regions, 0.6% in the generally allowed regions while 0.1% of the amino acid residues are in the disallowed regions. In all, the model was generally acceptable to employed for the purpose of this report.

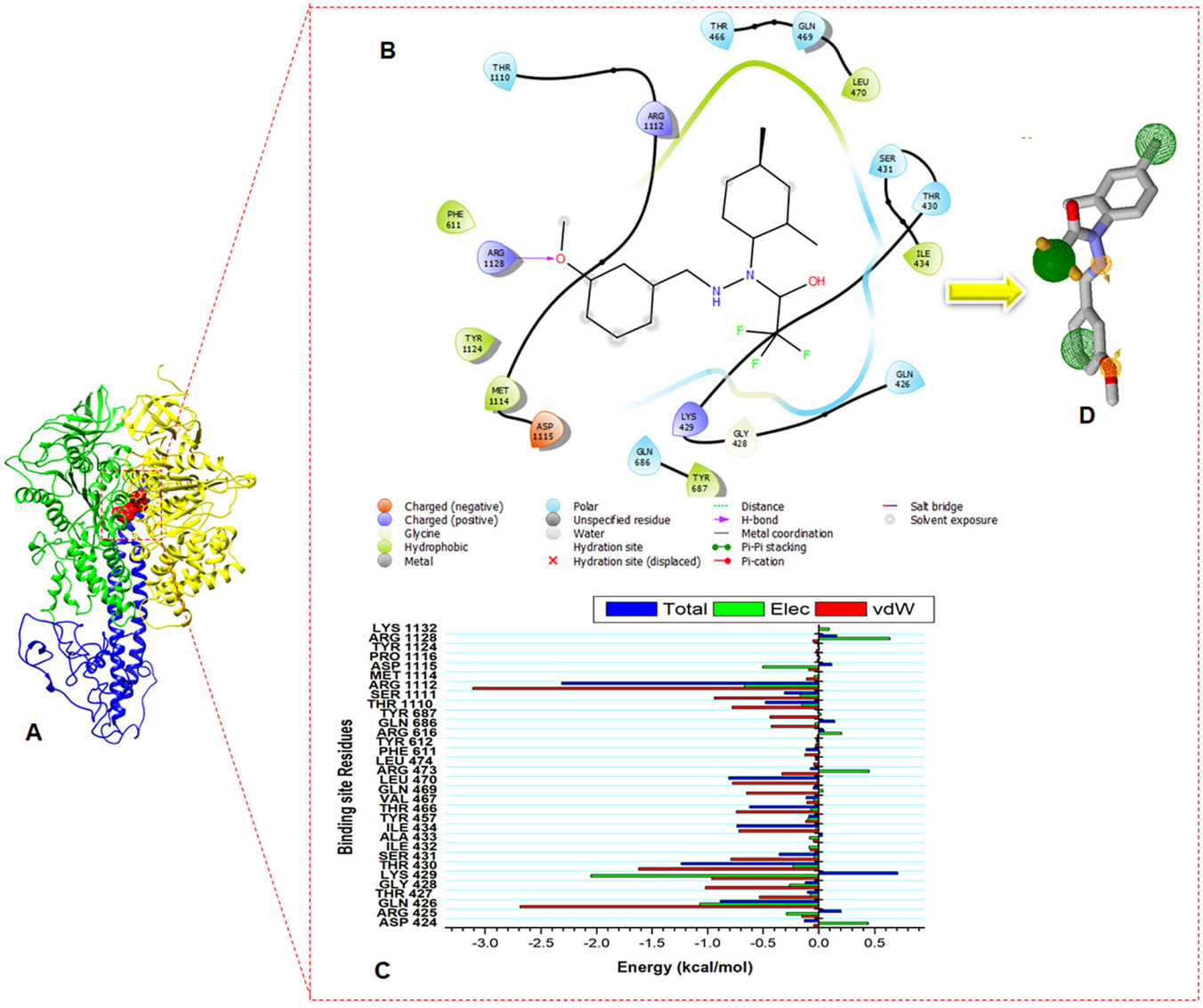

Fig. 1. Graphical representation of the procedure for the generation of the pharmacophore model in this study. A) 3D structure of ATP synthase in complex with J147. B) Residue interaction network of J147 and ATP synthase complex after 20 ns simulation. C) Per- residue energy decomposition plot of amino acid residues that contributed most to the interaction energy of J147 binding. D) 3D pharmacophore model (Green shows Hydrophobic interaction while yellow shows hydrogen bond donor/acceptor) generated in ZINCPharmer based on the essential interactions in the J147-ATP synthase after 20 ns simulation which was used for screening the ZINC database to obtain the top hit compounds. (For interpretation of the references to colour in this figure legend, the reader is referred to the web version of this article.)

Per-residue energy decomposition (PRED) pharmacophore model

In this study, a pharmacophore model was achieved via the per residue energy decomposition approach based on the energetic involvement of key active site residues. The structural features of the α-F1-ATP synthase and chemical characteristics of the J147 were employed in the construction of a pharmacophore model by focusing on J147 moieties that played critical roles in active site interactions.

Fig. 1 shows per-residue energy decomposition analysis after 20 ns pre-molecular dynamics simulation and ligand interaction for *m*ATP synthase and J147. Accordingly, Arg1112 (−2.312 kcal/mol), Thr430 (−1.239 kcal/mol), Gln426 (−0.886 kcal/mol) and Leu470 (−0.809 kcal/mol) to be the highest energy contributing residues of the α-ATP5A domain. Arg1128 donated hydrogen atom to the oxygen atom of the hexene ring of the ligand. However, based on per-residue plot, Arg1128 showed unfavourable total energy contribution toward J147 (0.164 kcal/mol). J147 displayed a good number of hydrophobic interactions with six residues of ATP synthase which are Ile434, Leu470, Phe611, Tyr687, Met1114, and Tyr1124. These features obtained from the ATP synthase-J147 complex was used to create the PRED-based pharmacophore on ZINCPharmer [42]. The model was then used to screen the ZINC database for potential drug compound against AD.

After the screening, 13 hits were obtained. These 13 hits were what was subjected to structure-based virtual screening that led to the obtaining of the 3 ligands with the highest docked binding energy. These 3 ligands were then subjected to molecular dynamics simulation together with the J147; the reference ligand for explore their potential as therapeutic agents in AD therapy.

Exploring the binding modes of top ranked hits at the ATP synthase allosteric site

The library of compounds that were generated from ZINC database were docked into the allosteric site of ATP synthase to examine their chemical and physical feasibility. The three top ranked molecules with the highest docking score were selected for further investigation. Based

Table 1
Docked poses of the lead compounds and their respective binding scores.

ZINC ID	Structure	Binding Energy (kcal/mol)
J147	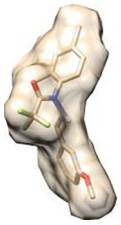	−7.5
ZINC04549531	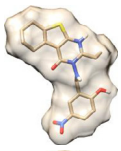	−8.8
ZINC70656000	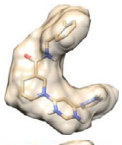	−8.7
ZINC70656005		−8.4

on the docking scores, hit compounds with the highest negative binding score; ZINC04549531 (−8.8 kcal/mol), ZINC70656000 (−8.7 kcal/mol) and ZINC70656005 (−8.4 kcal/mol) were picked as the respective top hits and further investigated to precisely determine the ligand-receptor stability as well as to examine their binding dynamics. Scoring functions from docking calculations attempt to reproduce experimental binding affinities, however most software are not consistent in giving the best prediction [43]. To conquer this challenge, the three best docked complexes were subjected to 100 ns molecular dynamic simulations. This facilitated validation of the binding affinities and also presented the avenue for further analysis of the effects of the lead compounds on enzyme's structural architecture upon their binding. Table 1 shows J147 and the best docked compounds with their corresponding docking scores.

Differential modulatory effects of the lead compounds on mATP synthase structure

The highest ranked compounds were subjected to 100 ns molecular dynamics simulation in order to check the convergence dynamic stability and to analyse the energetics of each complex. Trajectories generated from the simulated complexes were further analysed for C-α atom root mean square deviation (RMSD), C-α root mean-square fluctuation (RMSF) and C-α radius of gyration to reveal insights on the structural dynamics upon binding.

Monitoring the impacts of inhibitor binding on structural stability of ATP synthase

The stability of ATP synthase upon binding of the hits was examined and presented in Fig. 2 by computing the deviation of Ca atoms over the course of the simulation [44]. A high RMSD value suggests an increase in atomistic deviation which corresponds with a structurally unstable protein whereas a structure with a low RMSD value indicates a protein with a decrease in structural deviation, hence very stable [45,46]. All simulated systems equilibrated at approximately 30 ns with the exception of ZINC04549531 which attained convergence at approximately 50 ns. Following the attainment of convergence, all the systems maintained a relative stable trajectory until 100 ns time of the MD simulation. The average RMSD of J147 is 5.05 Å, that of ZINC04549531, ZINC70656000 and ZINC70656005 are 6.35 Å, 4.07 Å and 5.59 Å respectively. This implied that the binding of ZINC70656000 induced a more stable protein conformation in the ATP synthase relative to the other hits including J147.

Effects of inhibitor binding on structural flexibility and compactness of ATP synthase

The root mean square fluctuation gives insight into the flexibility of overall protein structure by estimating the fluctuation of each of the individual amino acids that make up the protein [47,48]. As building blocks of amino acids, their conformational dynamics will play critical role in the overall function of the protein [49,50]. As such, we calculated the RMSF of the amino acids that constitute *m*ATP synthase upon binding of each hit and J147 to monitor their impact on the conformations dynamics. As shown in Fig. 3A, the J147 bound system showed the highest residue fluctuation with an average RMSF of 15.06 Å relative to the simulated hits. Among the hits, ZINC70656005 induced the highest fluctuation of residues with an average of RMSF of 13.66 Å whiles ZINC70656000 exhibited the least level residue disorientations with an average RMSF of 9.21 Å. ZINC04549531 exhibited moderate levels of fluctuations with an average RMSF of 10.33 Å. Taken together, the observed flexibility in the protein structure of *m*ATP synthase indicated that the binding of the hits induced a consistent residual perturbation and structural disorientation much similar to J147 which is suggestive that the mechanism of action of these hits could be similar to that of the experimentally proven J147.

To further explore the conformational dynamics of ATP synthase upon binding of the hits relative to J147, we monitored the compactness of the entire structure of *m*ATP synthase over the simulation period since how tight or lose a protein structure is could interfere with its physiological properties. In doing so, we calculated the radius of gyration (RoG) of the Ca atoms of ATP synthase which measures the moment of inertia of each of the Ca atoms [51]. As shown in Fig. 3B, ZINC70656005 induced the highest RoG relative to all systems including J147 with an average value of 37.21 Å. The higher RoG implied the binding of ZINC70656005 resulted in a looser ATP synthase conformation relative to the rest of the systems. The lowest RoG and the corresponding most compact ATP synthase was observed in the ZINC70656000 bound conformation with an average value of 36.33 Å. Although the rest of the systems exhibited much lower RoG values relative to ZINC70656005, the relative difference amongst them was minimal. ZINC04549531 and J147 exhibited an average RoG value of 36.52 Å and 36.62 Å. Overall, the with the exception ZINC70656005, the mechanism by which these inhibitors induced compactness on ATP synthase could be assumed to be similar.

Comparative binding free energy analysis of hit compounds

We performed thermodynamic calculations to gain quantitative insights into the mechanistic binding profiles of the potential inhibitors relative to J147 towards ATP synthase using the MM/PBSA approach. As shown in Table 2, J147 exhibited a favourable total free binding energy of −44.71 kcal/mol with ATP synthase. Amongst the potential inhibitors, ZINC04549531 recorded the highest total binding free energy of −62.39 followed closely by ZINC70656000 with −62.10 kcal/mol. The high binding free energy observed could be attributed to the increased van der Waals and electrostatic energy showcased in the calculations. ZINC70656005 showed the lowest binding free energy of −26.68 ± 0.31 kcal/mol amongst all three potential compounds. The higher binding free energy of ZINC04549531 and ZINC70656000 than J147 suggests they could exhibit better inhibitory activity than J147 upon further experimental validation.

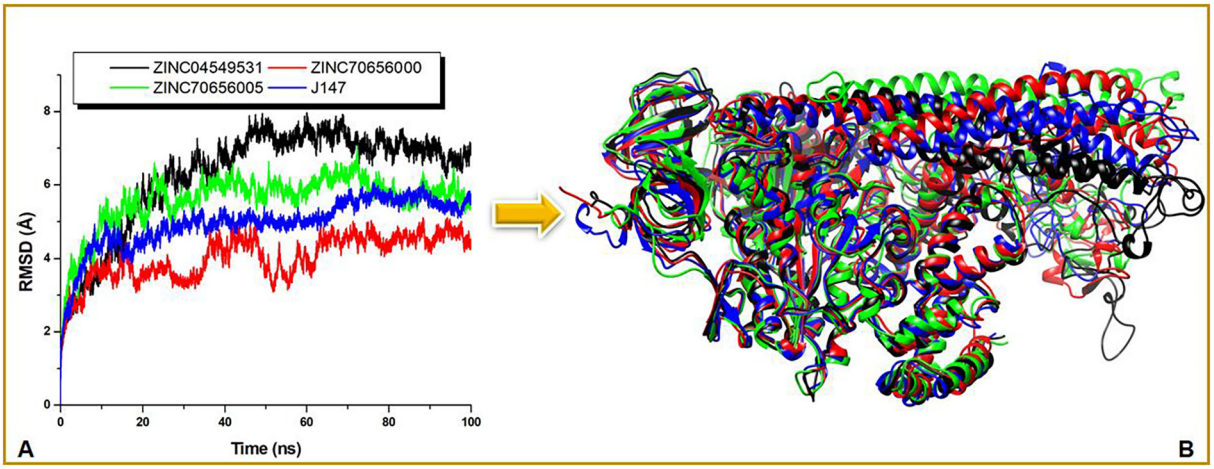

Fig. 2. Comparative analysis of the stability state of the four studied systems. A) Comparative RMSD plot of Ca atoms of J147, ZINC04549531, ZINC70656000 and ZINC70656005 and ATP synthase complex. B) Is the superimposed structure of the four protein systems showing the deviation of the respective protein structure form each other. The protein structures are coloured to tally with the respective colour of their individual trajectory on the plot.

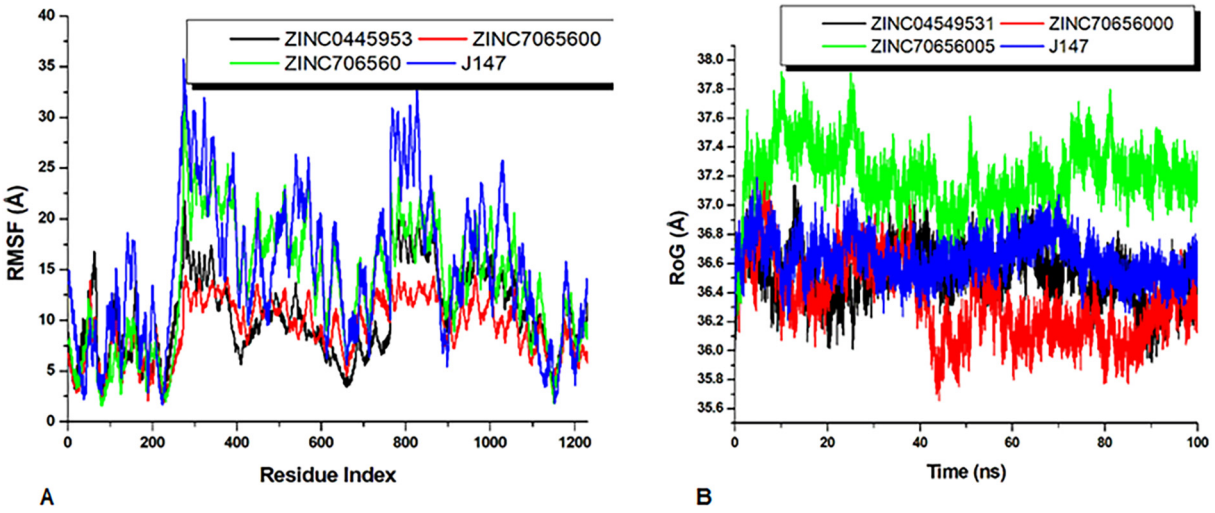

Fig. 3. Conformational dynamics of ATP synthase upon binding of the hits and J147. A) RMSF plot of Cα atoms of J147, ZINC04549531, ZINC70656000 and ZINC70656005 and ATP synthase complex. B) RoG plot of Cα atoms of J147, ZINC04549531, ZINC70656000 and ZINC70656005 and ATP synthase complex.

Comparative exploration of energy profiles of binding residues after 100 ns MD simulation

In order to provide more insights into the contribution of each residue to the binding of the three hits, we performed a per-residue based energy decomposition calculation to reveal crucial residues to their activity. This permitted a further understanding of their respective binding at the atomistic level. Residues with energies more than −1 kcal/mol were considered very crucial to the overall binding of the particular compound in question. Top contributing residues for each of the hits estimated from the per-residue energy decomposition are summarised in Table 3. Numbering of residues are based on amino acid numbering obtained from system preparation, however, corresponding the corresponding PDB residue numbering is included in the Supplementary Table S2.

The unravelling of these essential residues provides a clearer atomistic perspective on the possible activity of these potential allosteric inhibitors of *m*ATP synthase. It was interesting to note that many of the crucial residues involved in the binding of the hits were recurring amongst all the hits which suggests that these hits could have similar mechanism of binding and potential inhibitory activity. Notable among such residues were Gln426 which was maintained prominence across

Table 2
Summary of free-binding energy contributions of the ATP synthase-ligand systems.

Systems	Energy components (kcal/mol)				
	ΔE_{vdw}	ΔE_{ele}	ΔG_{gas}	ΔG_{sol}	ΔG_{bind}
J147	−38.12 ± 0.10	−71.24 ± 1.35	−84.95 ± 1.32	120.24 ± 1.23	−44.71 ± 0.40
ZINC04549531	−62.92 ± 0.12	4.66 ± 1.08	−57.25 ± 1.17	−5.14 ± 8.35	−62.39 ± 0.47
ZINC70656000	−48.52 ± 0.22	−5.95 ± 0.64	−54.47 ± 0.67	−7.63 ± 0.57	−62.10 ± 0.48
ZINC70656005	−37.84 ± 0.26	−456.37 ± 1.81	−494.21 ± 1.83	467.52 ± 1.75	−26.68 ± 0.31

ΔE_{ele} = electrostaic energy; ΔE_{vdw} = van der Waals energy; ΔG_{bind} = total binding free energy; ΔG_{sol} = solvation free enegry ΔG_{gas} = gas phase free energy.

Table 3
Energies and corresponding residues key to the binding of respective hit compounds on mATP synthase.

J147 (kcal/mol)	ZINC04549531 (kcal/mol)	ZINC70656000 (kcal/mol)	ZINC70656005 (kcal/mol)
Arg1112(−2.312)	Gln426 (−7.728)	Gln426 (−6.637)	Asp523 (−11.114)
Thr430(−1.239)	Arg1112 (−3.727)	Arg1112 (−6.148)	Gly428 (−3.208)
Gln426(−0.886)	Tyr687 (−1.99)	Arg425 (−5.428)	Thr427 (−2.265)
	Gln686 (−1.845)	Thr1110 (−2.115)	Gln426 (−1.036)
		Lys429 (−2.344)	Ser431 (−1.022)

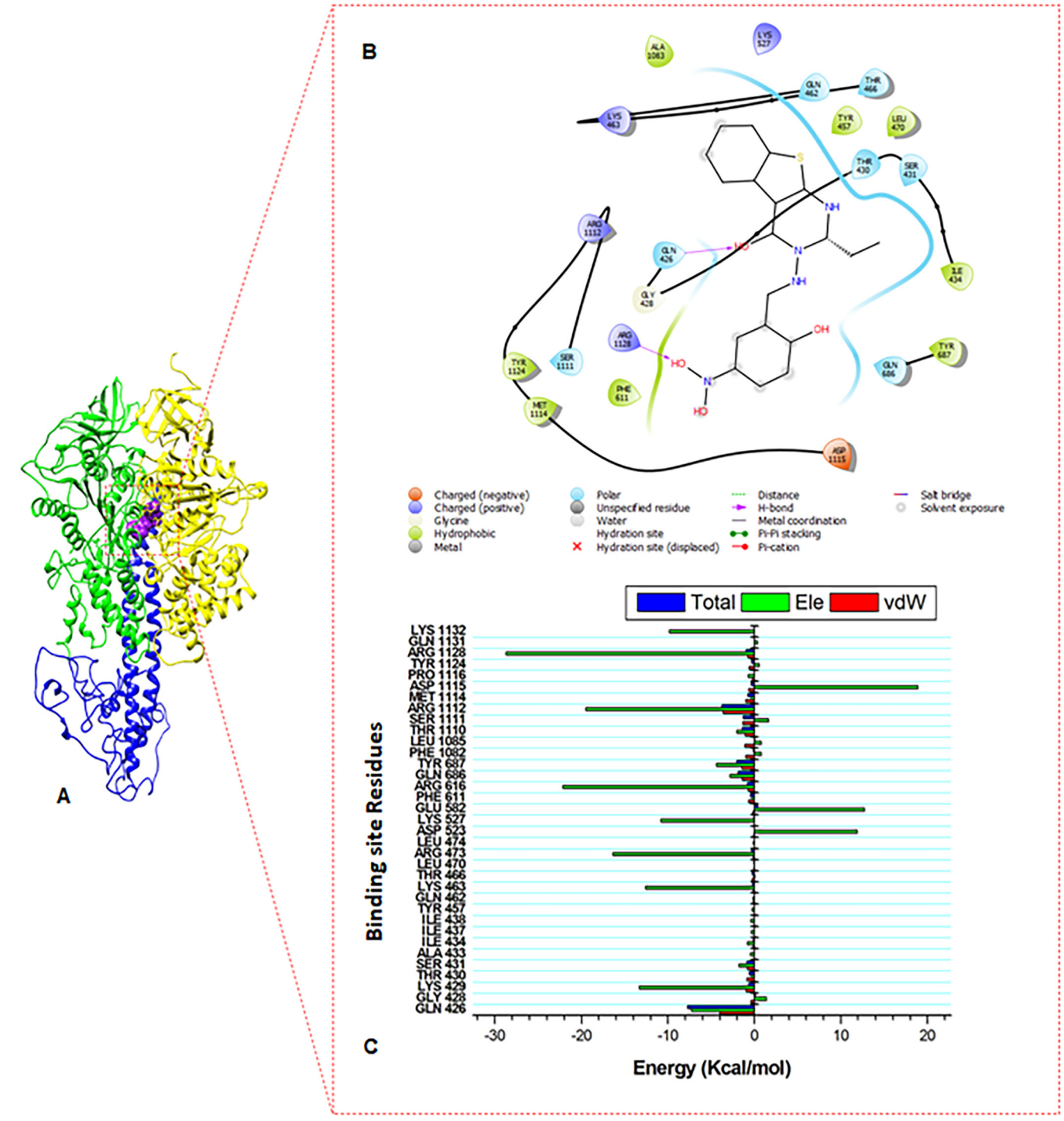

Fig. 4. Energy contributions and residue interaction plot of ATP synthase-ZINC04549531 complex. A) 3D structure of ATP synthase in complex with the ZINC04549531. B) ZINC04549531-ATP synthase interaction C) Per-residue energy decomposition plot showing the amino acid residues that contributed most to the binding of ZINC04549531.

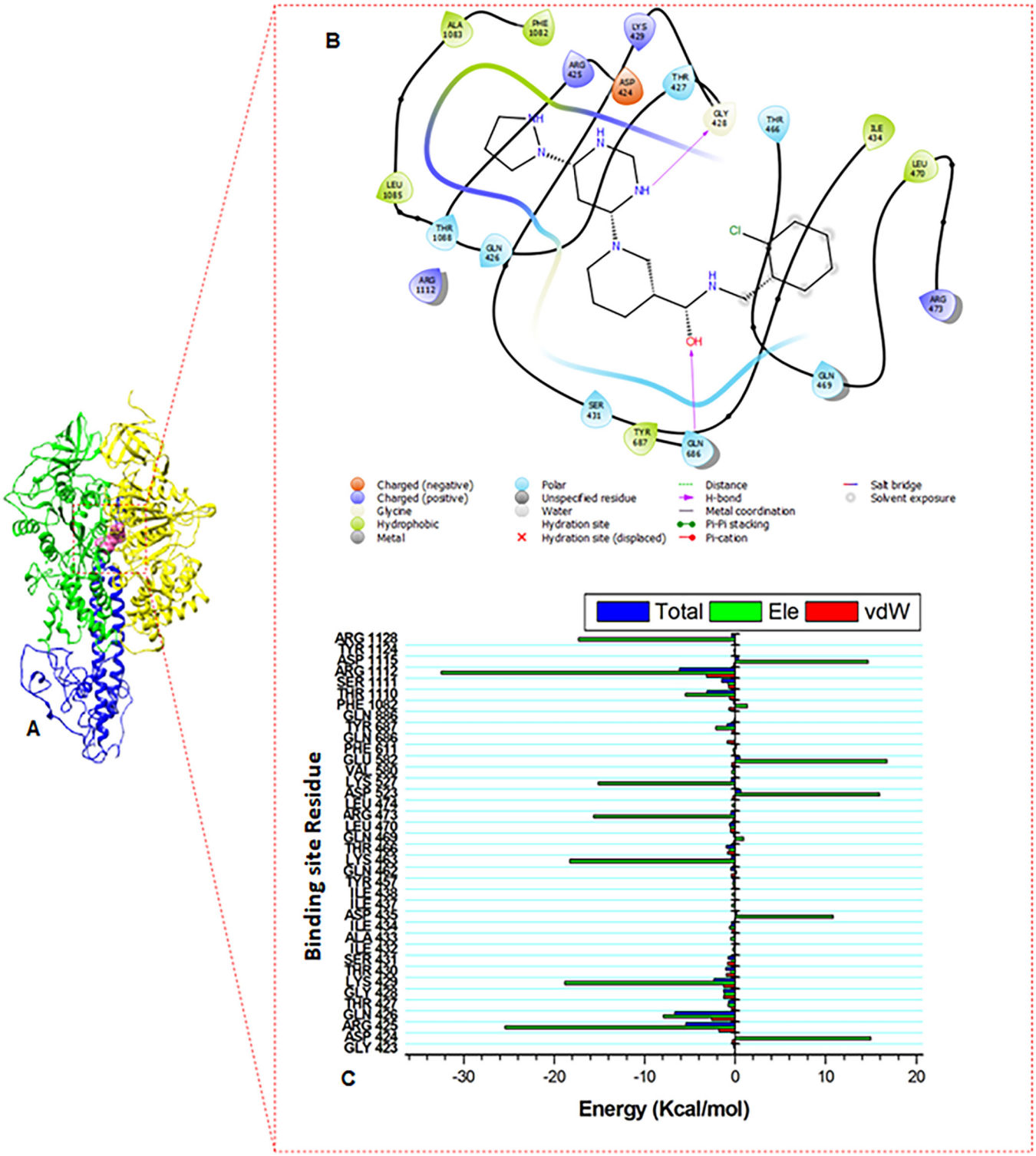

Fig. 5. Energy contribution and residue interaction plot of ATP synthase- ZINC70656000 complex. A) 3D structure of ATP synthase in complex with the ZINC70656000. B) ZINC04549531-ATP synthase interaction C) Per-residue energy decomposition plot showing the amino acid residues that contributed most to the binding of ZINC70656000.

all systems and Arg1112 which also recurred in all other systems except ZINC70656005. These key residues together with other residues which formed hydrophobic interactions as shown in Figs. 4–6 collectively contributes to the total binding of the respective inhibitors.

Comparative assessment of the drug-likeness of hit compounds relative to J147

With several reports available in literature, highlighting the therapeutic prowess of J147, there are few to no reports of side effects of J147. Using the online platform, SwissADME, we showcased the drug-worthy properties of all the hits as well as J147 to ascertain their safety

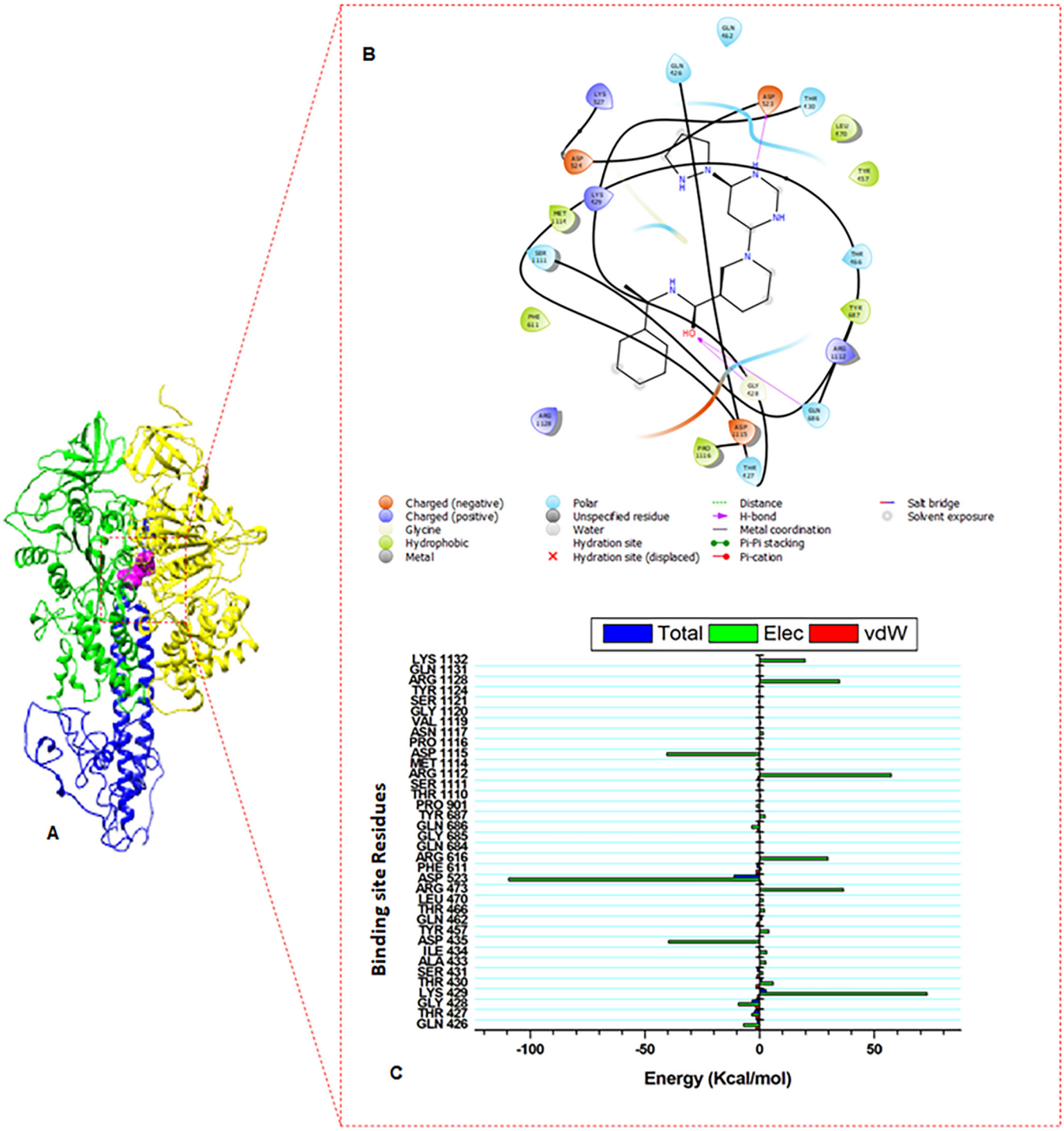

Fig. 6. Energy contribution and residue interaction plot of ATP synthase-ZINC70656005 complex. A) 3D structure of ATP synthase in complex with the ZINC70656005. B) ZINC70656005-ATP synthase interaction C) Per-residue energy decomposition plot showing the amino acid residues that contributed most to the binding of ZINC70656005.

as presented in Table 4. More so, the therapeutic success of these hits is dependent on their pharmacokinetic properties, potency, selectivity and safety, hence the revelation of these properties for the hits will be relevant for further experimental exploration. A crucial pharmacokinetic property to consider in analysing the success of these hits and any chemical agent in general is their bioavailability. The bioavailability of the potential hits and J147 takes into consideration the amount of administered doses of these agents that will get absorbed [52,53]. A look at the lipophilicity of the of the studied compounds was also an important factor in assessing the drug-like property of our studied compounds including J147. An idea of their respective lipophilicity gives an insights into the permeability, solubility or their respective hepatic clearance [54]. Typically, a small molecule inhibitor with a LogP ranging from 2 to 3 is usually considered to have a favourable permeability and a corresponding promising first-pass clearance [43,55]. As such, the lipophilicity of our hits and J147 were also provided to further support the potential efficacy in addition possible experimental validation. Apart from ZINC04549531 which had a LogP of 2.70, all other hits including J147 showcased a slightly higher LogP above 3.0 suggesting less favourable permeability and first-pass

Table 4
Comparative analyses of drug-likeness of the screened compounds with that of the experimental J147.

Parameters	J147	ZINC04549531	ZINC70656000	ZINC70656005
Molecular formula	C18H17F3N2O2	C19H17N4O4S	C20H21ClN6O	C21H24N6O
Molecular weight g/mol	350.33	397.43	396.87	376.45
Lipophilicity (iLog*P*)	3.52	2.70	3.31	3.39
Water soluble	Moderately Soluble	Moderately soluble	Moderately soluble	Soluble
GIT absorption	High	Low	High	High
BBB permeability	Yes	No	Yes	Yes
Bioavailability score	0.55	0.56	0.55	0.55
Synthetic accessibility	2.74	3.69	3.50	3.81
Druglikeness (Lipinski)	Yes	Yes	Yes	Yes
'Boiled-Egg' method summary	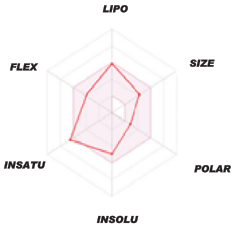		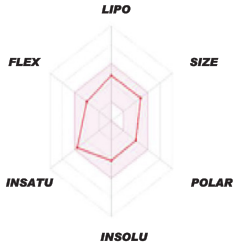	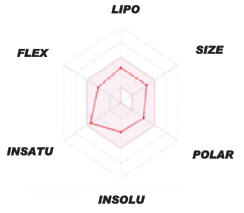

clearance. The compatibility of the hits and J147 with the Lipinski's rule of five [56] were also evaluated and showcased in the table to further augment earlier properties provided that support their potential as allosteric inhibitors of ATP synthase. All hits and J147 obeyed all Lipinski's rule of five, confirming their potential drug-likeness which could be further explored and validated by experimental procedures. Again, with the exception of ZINC04549531 which was shown to have low gastrointestinal absorption (GIT) and an inability to cross the blood brain barrier, all other hits including J147 exhibited high GIT absorption, a demonstrable permeability of the blood brain barrier as well solubility in water.

Conclusion

Alzheimer's disease is a slow but progressive disease that destroys memory and other important mental functions. The limited number as well as possible associated side effects of current therapeutic options in AD necessitates a continuous search for more viable therapeutic alternatives. Based on the allosteric inhibitory property of J147 against α-F1-ATP synthase, this study employs computational methods to identify potential anti-AD inhibitors with similar or enhanced inhibitory properties as J147 which can be further explored towards the design of novel α-F1-ATP synthase inhibitors. A pharmacophore based virtual screening was performed to identify three new potential allosteric inhibitors of ATP synthase; ZINC04549531, ZINC70656000 and ZINC70656005, which possessed similar binding and allosteric site interaction mechanisms as the known AD therapeutic agent, J147. Further exploration of the pharmacokinetic analysis of these compounds revealed highly favourable properties, such as alignment with the Lipinski's rule of five, permeability of the blood brain barrier and a high GIT absorption for ZINC70656000 and ZINC70656005. The previous experimental validation of J147 coupled with similarity in binding modes and pharmacokinetic properties of the identified hits from our pharmacophore based virtual screening, a further experimental validation of our finding of our potential hits could lead the way in the design of new allosteric inhibitors of ATP synthase towards AD therapy.

Declaration of Competing Interest

The authors declare no conflict of interest.

Acknowledgement

The authors appreciate the College of Health Sciences, University of KwaZulu-Natal for their infrastructural and financial support. In the same manner, we thank the Center for High Performance Computing, (CHPC, www.chpc.ac.za) Cape-Town for providing computational resources.

Appendix A. Supplementary data

Supplementary data to this article can be found online at https://doi.org/10.1016/j.mehy.2019.109277.

References

[1] Guerreiro R, Bras J. The age factor in Alzheimer's disease. Genome Med 2015;7:106.
[2] Niccoli T, Partridge L. Ageing as a risk factor for disease. Curr Biol 2012;22(17):R741–52.
[3] Mawuenyega KG, Sigurdson W, Ovod V, Munsell L, Kasten T, Morris JC, et al. Decreased clearance of CNS beta-amyloid in Alzheimer's disease. Science 2010;330(6012):1774.
[4] Hardy J, Selkoe DJ. The amyloid hypothesis of Alzheimer's disease: progress and problems on the road to therapeutics. Science 2002;80-:353–6.
[5] Cummings JL, Cole G. Alzheimer disease. JAMA 2002;287(18):2335–8.
[6] Yiannopoulou KG, Papageorgiou SG. Current and future treatments for Alzheimer's disease. Ther Adv Neurol Disord. 2013;6(1):19–33.
[7] Casey DA, Antimisiaris D, O'Brien J. Drugs for Alzheimer's disease: are they effective? P T. 2010;35(4):208–11.
[8] Chen Q, Prior M, Dargusch R, Roberts A, Riek R, Eichmann C, et al. A novel neurotrophic drug for cognitive enhancement and Alzheimer's disease. Iijima KM, editor. PLoS One 2011;6(12):e27865.
[9] Prior M, Dargusch R, Ehren JL, Chiruta C, Schubert D. The neurotrophic compound J147 reverses cognitive impairment in aged Alzheimer's disease mice. Alzheimers Res Ther 2013;5(3):25.
[10] Currais A, Goldberg J, Farrokhi C, Chang M, Prior M, Dargusch R, et al. A comprehensive multiomics approach toward understanding the relationship between aging and dementia. Aging (Albany NY) 2015;7(11):937–55.
[11] Goldberg J, Currais A, Prior M, Fischer W, Chiruta C, Ratliff E, et al. The mitochondrial ATP synthase is a shared drug target for aging and dementia. Aging Cell 2018.
[12] Prior M, Goldberg J, Chiruta C, Farrokhi C, Kopynets M, Roberts AJ, et al. Selecting for neurogenic potential as an alternative for Alzheimer's disease drug discovery. Alzheimer's Dement 2016;12(6):678–86.
[13] Jonckheere AI, Smeitink JAM, Rodenburg RJT. Mitochondrial ATP synthase: architecture, function and pathology. J Inherit Metab Dis 2012;35(2):211–25.
[14] Symersky J, Osowski D, Walters DE, Mueller DM. Oligomycin frames a common drug-binding site in the ATP synthase. Proc Natl Acad Sci USA 2012;109(35):13961–5.
[15] Racker E. A mitochondrial factor conferring oligomycin sensitivity on soluble mitochondrial ATPase. Biochem Biophys Res Commun 1963;10(6):435–9.
[16] Ahmad Z, Laughlin TF. Medicinal chemistry of ATP synthase: a potential drug target of dietary polyphenols and amphibian antimicrobial peptides. Curr Med Chem

2010;17(25):2822–36.
[17] Nam K, Pu J, Karplus M. Trapping the ATP binding state leads to a detailed understanding of the F1-ATPase mechanism. Proc Natl Acad Sci USA 2014;111(50):17851–6.
[18] Ahmad Z, Okafor F, Azim S, Laughlin TF. ATP synthase: a molecular therapeutic drug target for antimicrobial and antitumor peptides. Curr Med Chem 2013;20(15):1956–73.
[19] Lu P, Lill H, Bald D. ATP synthase in mycobacteria: Special features and implications for a function as drug target. Biochim Biophys Acta - Bioenergy 2014;1837(7):1208–18.
[20] Kalita JM. Advances in computer aided drug design;2015.
[21] Ramharack P, Soliman MES. Zika virus NS5 protein potential inhibitors: an enhanced *in silico* approach in drug discovery. J Biomol Struct Dyn 2018;36(5):1118–33.
[22] Agoni C, Ramharack P, Soliman MES. Allosteric inhibition induces an open WPD-loop: a new avenue towards glioblastoma therapy. RSC Adv 2018;8(70):40187–97.
[23] Daina A, Michielin O, Zoete V. iLOGP: a simple, robust, and efficient description of *n* -octanol/water partition coefficient for drug design using the GB/SA approach. J Chem Inf Model 2014;54(12):3284–301.
[24] Daina A, Zoete V. A BOILED-egg to predict gastrointestinal absorption and brain penetration of small molecules. ChemMedChem 2016;1117–21.
[25] Abrahams JP, Leslie AGW, Lutter R, Walker JE. Structure at 2.8 Â resolution of F1-ATPase from bovine heart mitochondria. Nature 1994.
[26] Ramharack P, Soliman MES. Zika virus drug targets: a missing link in drug design and discovery – a route map to fill the gap. RSC Adv 2016;6(73):68719–31.
[27] Munsamy G, Ramharack P, Soliman MES. Egress and invasion machinery of malaria: an in-depth look into the structural and functional features of the flap dynamics of plasmepsin IX and X. RSC Adv 2018;8(39):21829–40.
[28] Laskowski RA, MacArthur MW, Moss DS, Thornton JM. IUCr. PROCHECK: a program to check the stereochemical quality of protein structures. J Appl Crystallogr 1993;26(2):283–91.
[29] Lovell SC, Davis IW, Arendall WB, de Bakker PIW, Word JM, Prisant MG, et al. Structure validation by Cα geometry: ϕ, ψ and Cβ deviation. Proteins Struct Funct Bioinforma 2003;50(3):437–50.
[30] Eisenberg D, Lüthy R, Bowie JU. VERIFY3D: assessment of protein models with three-dimensional profiles. Methods Enzymol 1997;277:396–404.
[31] Yang Z, Lasker K, Schneidman-Duhovny D, Webb B, Huang CC, Pettersen EF, et al. UCSF Chimera, MODELLER, and IMP: an integrated modeling system. J Struct Biol 2012;179(3):269–78.
[32] Trott O, Olson AJ. AutoDock Vina: improving the speed and accuracy of docking with a new scoring function, efficient optimization, and multithreading. J Comput Chem. 2010;31(2):455–61.
[33] Hanwell MD, Curtis DE, Lonie DC, Vandermeerschd T, Zurek E, Hutchison GR. Avogadro: an advanced semantic chemical editor, visualization, and analysis platform. J Cheminform 2012;4(8).
[34] Maier JA, Martinez C, Kasavajhala K, Wickstrom L, Hauser KE, Simmerling C. ff14SB: improving the accuracy of protein side chain and backbone parameters from ff99SB. J Chem Theory Comput 2015;11(8):3696–713.
[35] Wang J, Wang W, Kollman PA, Case DA. Antechamber, An Accessory Software Package For Molecular Mechanical Calculations Correspondence to. Journal of Chemical Information and Computer Sciences.
[36] Harvey MJ, De Fabritiis G. An implementation of the smooth particle mesh Ewald Method on GPU hardware. J Chem Theory Comput 2009;5(9):2371–7.
[37] Genheden S, Ryde U. The MM/PBSA and MM/GBSA methods to estimate ligand-binding affinities. Expert Opin Drug Discov 2015;10(5):449–61.
[38] Forli S, Huey R, Pique ME, Sanner MF, Goodsell DS, Olson AJ. Computational protein–ligand docking and virtual drug screening with the AutoDock suite. Nat Protoc 2016;11(5):905–19.
[39] Sanner MF, Olson AJ, Spehner JC. Reduced surface: an efficient way to compute molecular surfaces. Biopolymers 1996;38(3):305–20.
[40] Morris GM, Huey R, Lindstrom W, Sanner MF, Belew RK, Goodsell DS, et al. AutoDock4 and AutoDockTools4: automated docking with selective receptor flexibility. J Comput Chem 2009;30(16):2785–91.
[41] Pettersen EF, Goddard TD, Huang CC, Couch GS, Greenblatt DM, Meng EC, et al. UCSF Chimera – a visualization system for exploratory research and analysis. J Comput Chem 2004;25(13):1605–12.
[42] Koes DR, Camacho CJ. ZINCPharmer: pharmacophore search of the ZINC database. Nucl Acids Res 2012;40(Web Server issue). W409-14.
[43] Ncube NB, Ramharack P, Soliman MES. An “All-In-One” pharmacophoric architecture for the discovery of potential broad-spectrum anti-flavivirus drugs. Appl Biochem Biotechnol 2018;185(3):799–814.
[44] Ndagi U, Mhlongo NN, Soliman ME. The impact of Thr91 mutation on c-Src resistance to UM-164: molecular dynamics study revealed a new opportunity for drug design. Mol BioSyst 2017;13(6):1157–71.
[45] Pitera JW. Expected distributions of root-mean-square positional deviations in proteins. J Phys Chem B 2014;118(24):6526–30.
[46] Olotu FA, Soliman MES. From mutational inactivation to aberrant gain-of-function: unraveling the structural basis of mutant p53 oncogenic transition. J Cell Biochem 2018;119(3):2646–52.
[47] Bornot A, Etchebest C, De Brevern AG. Predicting protein flexibility through the prediction of local structures. Proteins Struct Funct Bioinforma 2011;79(3):839–52.
[48] Machaba KE, Mhlongo NN, Soliman MES. Induced mutation proves a potential target for TB therapy: a molecular dynamics study on LprG. Cell Biochem Biophys 2018;76(3):345–56.
[49] Spassov VZ, Yan L, Flook PK. The dominant role of side-chain backbone interactions in structural realization of amino acid code. ChiRotor : a side-chain prediction algorithm based on side-chain backbone interactions. Protein Sci 2007;16(3):494–506.
[50] Chaffey N, Alberts B, Johnson A, Lewis J, Raff M, Roberts K, Walter P. Molecular biology of the cell. 4th edn. Ann Bot 2003;91(3). 401–401.
[51] Bhakat S, Martin AJM, Soliman MES. An integrated molecular dynamics, principal component analysis and residue interaction network approach reveals the impact of M184V mutation on HIV reverse transcriptase resistance to lamivudine. Mol BioSyst 2014;10(8):2215–28.
[52] Toutain PL, Bousquet-mé Lou A. Bioavailability and its assessment.
[53] Kumar R, Sharma A, Varadwaj PK. A prediction model for oral bioavailability of drugs using physicochemical properties by support vector machine. J Nat Sci Biol Med 2011;2(2):168–73.
[54] Liu X, Testa B, Fahr A. Lipophilicity and Its Relationship with Passive Drug Permeation.
[55] Ahmed SSSJ, Ramakrishnan V. Systems biological approach of molecular descriptors connectivity: optimal descriptors for oral bioavailability prediction. PLoS One 2012;7(7).
[56] Lipinski CA, Lombardo F, Dominy BW, Feeney PJ. Experimental and computational approaches to estimate solubility and permeability in drug discovery and development setting. Adv Drug Deliv Rev 2012;64:4–17.